The HMI Ring-Diagram Pipelines: A Status Report

R.S. Bogart[1], C.S. Baldner[1], S. Basu[2], D.A. Haber[3], R. Howe[4], I. González Hernández[5], F. Hill[5], K. Jain[5], R. Komm[5], M.C. Rabello-Soares[1], S. Tripathy[5]

[1]Stanford University; [2]Yale University; [3]University of Colorado; [4]University of Birmingham; [5]National Solar Observatory

Abstract

The HMI analysis pipeline for determination of sub-surface flows has been running for nearly one year, and virtually all HMI Doppler data from the beginning of the mission have been analyzed. Over 3.5 million local-area power spectra of regions of various sizes have been produced and fitted, and inversions for the depth structure of flows have been produced for over 130,000 of the larger regions. The pipeline for determination of the sub-surface thermal structure is still under active development, with test results available for analysis for a number of strong active regions. We describe the ring-diagram pipelines, report on their performance as part of the overall HMI data analysis pipeline, describe the data products available, and discuss outstanding problems and issues for further development.

Pipeline Descriptions

The HMI ring-diagram pipelines implement techniques of plane-wave local helioseismic analysis to determine spatially-resolved sub-photospheric fluid flow fields and thermal structures on a synoptic scale, and in the neighborhood of targeted regions of interest. Two pipelines have been designed, a synoptic pipeline for regular sampling on a global scale, and a target pipeline for measurement of anomalies in the flows and thermal structure associated with active regions. Here we describe only the synoptic pipeline, which is fully operational; both pipelines share common elements.

The synoptic pipeline processing consists of the following steps:

- **Assessment of data quality and coverage:** The availability of observables data to be analyzed is regularly monitored, and when all data to be expected for the required time interval are available (typically within about 3.5 days of the end of the interval), the data are checked for quality. Most data can be accepted based on their automatically assigned quality mask, but occasional images are marked not to be used for processing based on anomalous statistics; most of these are in post-eclipse thermal recovery phases. If the fraction of available data, after automatic and tabulated image rejection, is lower than 0.7 of the possible data for the period to be analyzed, further analysis is not attempted.
- **Averaging of observables:** All acceptable images are averaged over a period equal to one-third of a Carrington rotation (~9 d). Such averages are produced six times per rotation, at times centered on central meridian longitudes of 360°, 300°, *etc.* The averages are used for detrending of the individual images, in order to remove first-order spatial field effects. In the case of Doppler data, the principal observable, the radial component of the spacecraft velocity is subtracted from the individual Dopplergrams prior to averaging.
- **Target generation:** The synoptic pipeline is run for three sets of region sizes (diameter 5°, 15°, and 30°) in tiles overlapped by half their extent in latitude and approximately the same arc distance in longitude, and extending to 80° from disc center. Because of the annual variation of 14°.5 in heliographic latitude of SDO, different heliographic coordinates are accessible at different times. Three different target sets are used for each set of tiles, one each for $B_0 < -3°.625$, $|B_0| \le 3°.625$, and $B_0 > 3°.625$ (Fig. 1). Not all regions can be analyzed all of the time: only 65 of the possible 73 30° regions, 261 of the 307 15° ones, and 2481 of the 3007 5° ones. The others are analyzed either 9 or 3 months per year.
- **MAI calculation:** It is useful to determine a Magnetic Activity Index (MAI) to characterize each of the regions analyzed. The MAI is calculated by applying (nearly) the same mapping, tracking, and apodization that will be used for the power spectra to the concurrent HMI magnetograms, and integrating the unsigned flux exceeding a threshold of 50G in the data cube. The MAI is set as a keyword for the corresponding tracked data cubes and derived products.
- **Mapping and tracking:** Each region is mapped from the original images under a Postel's (azimuthal equidistant) projection centred at its target Carrington coordinates for an interval approximately equal to the time over which it would rotate through its width; this implies tracking at the Carrington rate for periods of about 1/72, 1/24, and 1/12 of a rotation for the 5°, 15°, and 30° tiles respectively. The exact times are based on the HMI observing cadence of 45 s, and are equal to 768, 2304, and 4608 samples for the three pipelines — 9^h36^m, 28^h48^m, and 57^h36^m.
- **Power spectra** of the tracked mapped data cubes are calculated with a 3-d Fourier transform, for plane-wave analysis in the mapped coordinate system. The power spectra are apodized with a circular spatial function tapering from 1 at the target diameter to 0 at the half-width of the map, along with a very slight temporal taper.
- **Fitting of the spectra:** The power spectra are fit for the frequencies and various parameters using two independent approaches: a fast procedure (*rdfitf*) that fits with five parameters, and a more comprehensive one (*rdfitc*) that fits a thirteen-parameter model. All spectra are fit with *rdfitf*, but owing to the computational cost, *rdfitc* is run on all 5° tiles, but for the 15° and 30° tiles, only on those on the central meridian and equator.

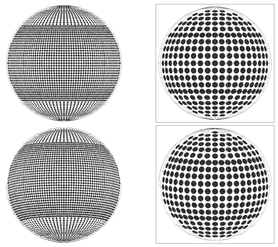

Fig. 1: Sample locations of the centers of the 5° tiles (left) and the 15° tiles (right) at different times of year, as projected on the solar disc. The locations at the top correspond to times when $B_0 < 3°.625$ (the heliographic grid is for $B_0 = 0$), those below for times when $|B_0| > 3°.625$. The spots are less than half the diameter of their corresponding regions, since the latter are overlapped. Note the increasing longitude spacing of the targets at high latitudes, in order to keep their actual spacing approximately uniform.

- **Flow inversions:** The wave advection parameters from the *rdfitf* fits for each 15° and 30° region are inverted against a solar model using a SOLA procedure to obtain estimates of the mean horizontal fluid velocity vector underlying the region, relative to the Carrington coordinate system, as a function of depth. The target depths go from the surface to 0.94 R_0 for the 30° tiles and 0.97 R_0 for the 15° tiles, both in steps of 0.001 R_0 (0.7 Mm).

Data Products

The following data series produced by the synoptic pipeline are permanently archived as they are created and "published", i.e. made available for distribution through the general JSOC export mechanisms and the Virtual Solar Observatory, and for automatic mirroring to other NetDRMS sites as requested. With the exception of the data averages and the flow inversions, individual records in the series are labeled by the Carrington rotation number, central meridian longitude at midtime of the analysis interval, Carrington longitude, and heliographic latitude of the region. (Stonyhurst longitude, though redundant, is also used as a prime key for ease of selection.)

Data averages
- **hmi.V_avg120:** averages of Doppler data over 1/3 Carrington rotation, sampled 6 per CR; labeled by Carrington rotation number and central meridian longitude at midtime

Mapped and tracked data cubes
- **hmi.rdVtrack_fd05:** 5° Doppler cubes on the synoptic grid tracked for 1/72 CR, sampled 72 per CR
- **hmi.rdVtrack_fd15:** 15° Doppler cubes on the synoptic grid tracked for 1/24 CR, sampled 24 per CR
- **hmi.rdVtrack_fd30:** 30° Doppler cubes on the synoptic grid tracked for 1/12 CR, sampled 12 per CR

Power spectra
Three-dimensional power spectra of the corresponding tracked cubes in $k_\ell k_r \omega$ space
- **hmi.rdVpspec_fd05**
- **hmi.rdVpspec_fd15**
- **hmi.rdVpspec_fd30**

Averaged power spectra
Averages over a Carrington rotation of the corresponding spectra at each Stonyhurst target location
- **hmi.rdVavgpspec_fd15:** labeled by Carrington rotation number, latitude, and Stonyhurst longitude
- **hmi.rdVavgpspec_fd30**

Ring fits
Fits to the corresponding power spectra using both *rdfitf* and *rdfitc* procedures: ASCII tables
- **hmi.rdVfitsf_fd05**
- **hmi.rdVfitsf_fd15**
- **hmi.rdVfitsf_fd30**
- **hmi.rdVfitsc_fd05**
- **hmi.rdVfitsc_fd15**
- **hmi.rdVfitsc_fd30**

Flow inversions
Depth inversions for flow fields of the corresponding *rdfitf* ring fits: ASCII tables
- **hmi.rdVflows_fd15_frame** sets of 281–284, sampled 24 per CR; labeled by Carrington rotation and CM longitude at midtime
- **hmi.rdVflows_fd30_frame** sets of 69, sampled 12 per CR

The following data series are being produced by the target pipeline. They are not permanently archived and generally disappear after a few months. They are available for analysis to science team members and can be provided to others by arrangement, through the same JSOC export mechanisms (JSOC2). Individual records in the series are labeled by a string identifier constructed from the target AR number and the region offset in latitude and longitude from the target

Mapped and tracked data cubes
- **hmi_test.rdVtrack_targ**

Power spectra
- **hmi_test.rdVpspec_targ**

Ring fits
- **hmi_test.rdVfitsc_targ**

Processing Status, Plans

18 complete rotations have been processed through the synoptic pipeline (Fig. 2). We are currently reviewing the pipeline process and data products for possible improvements. Final implementation of the target pipeline awaits further development of the inversion procedures, expected early next year. Test data have been produced for eleven active regions, including all of those that crossed central meridian during CR 2100.

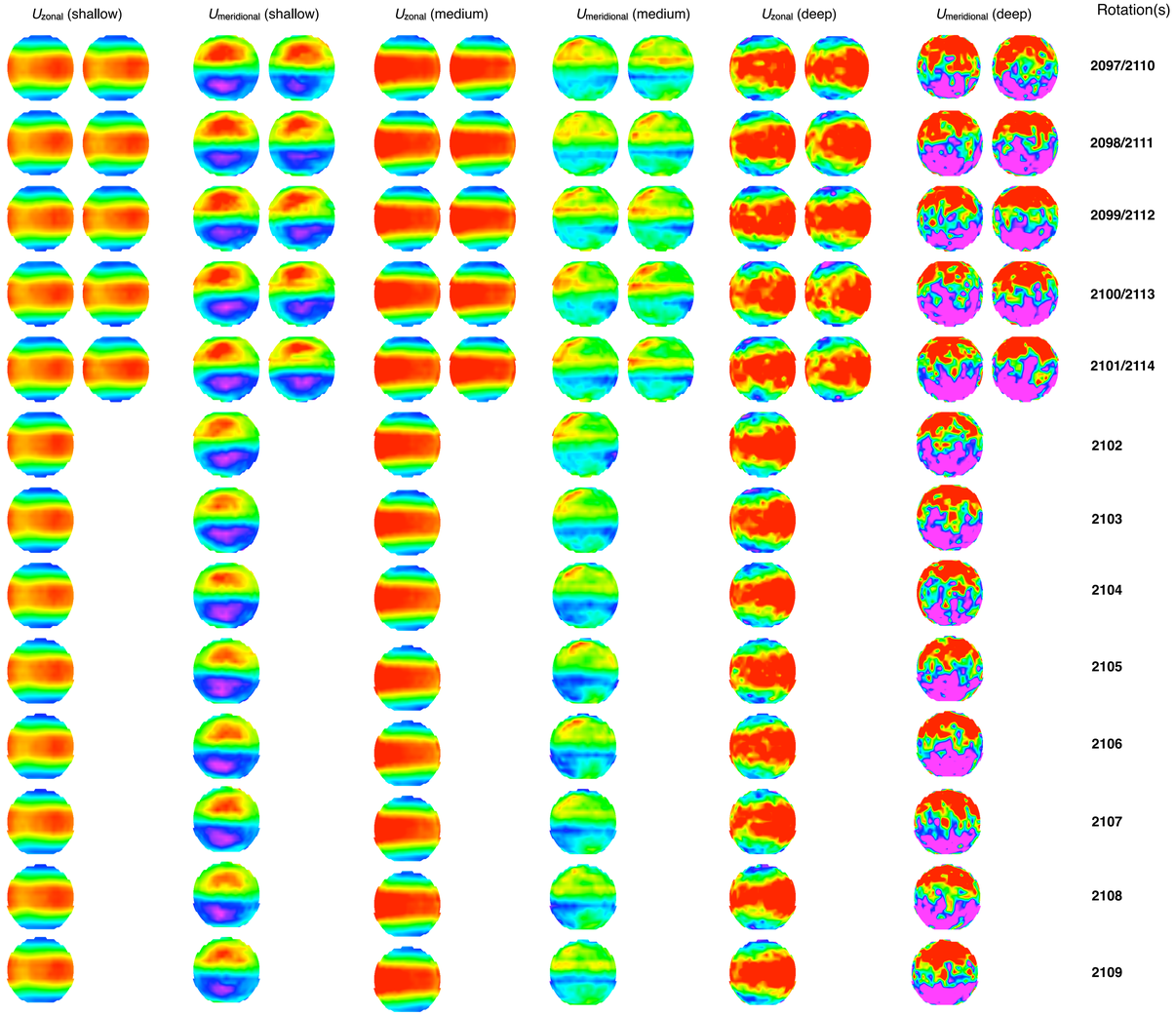

Fig. 3: Average flow parameters U_ℓ, U_r from the *rdfitc* fits to the averaged power spectra of the 15° tiles for each Carrington rotation over the observed solar disc (Stonyhurst coordinates). The parameters are shown averaged for all modes over three different ranges in the classical turning point value v/l: 2–4 (shallow), 9–11 (medium), and 18–24 (deep). Carrington rotations at about the same time of year are lined up next to each other in order to help identify annual contributions to the systematic variations such as might be caused by variation in the heliographic latitude of SDO or the apparent solar diameter. The color scale (violet to red) is the same for each set of images: it ranges from -200 to 0 m/s for the zonal flow parameter and ±30 m/s for the meridional flow parameter.

We have recently added two new data products to the synoptic pipeline, averages of the power spectra for the 15° and 30° tiles at each "disc position" (Stonyhurst coordinates) over the 24 or 12 samples respectively of a Carrington rotation. These averaged spectra are being used to help understand systematic effects in the ring spectra themselves (and the fitting procedures) that depend on observing geometry. It is expected that they will also be used to establish a baseline of reference frequencies to be used in structure inversions, since the averages have greatly enhanced signal to noise. All 18 Carrington rotations during which HMI has observed have been analysed, and the results for the flow parameters shown in Fig. 3 dramatically illustrate the systematic effects. The substantial east-west variation in the apparent differential rotation must certainly be an artifact. It is interesting that the systematic asymmetries are strongly dependent on the mode set, implying different variations with depth in the inverted flows. The differences are striking for the zonal flow, for which the east-west gradient actually reverses sign, but they are also clear in the meridional flow parameter as well. (Most estimates of meridional circulation have been based on fits along the central meridian only.) The dependence of these variations on mode set may be related to the dependence of the systematic east-west differences in mode frequency with frequency, as illustrated in Fig. 4. It has been suggested that long-term variations in the inferred flows may be due to the annual variation in observer B_0. There is some evidence of such an annual trend in the asymmetric structures, but it clearly does not account for most of the temporal variations. Some, particularly at lower latitudes, may also be caused by the overall increase in activity as well.

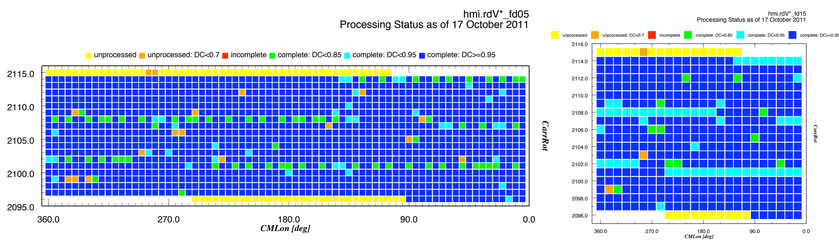

Fig. 2: Graphical representation of the current processing status of data products in the synoptic pipeline. "Complete" means that all records of all series for the corresponding Carrington time exist; "incomplete" means that some records for some of the series exist, typically because processing is going on at the time of the status report; "unprocessed" means that no tracked data cubes have been produced, and consequently none of the derived records. Times of low duty cycle, predominantly due to eclipses and spacecraft maneuvers supporting instrument calibrations, are noted in lighter blue and green. Ring-diagram results during these times may be less reliable, though this effect has not yet been quantified. Only the status for the 5° and 15° tiles is shown; the 30° tiles have similar coverage, except that they have experienced no times for which the duty cycle fell below 0.7. Status reports are updated weekly and available at *http://hmi.stanford.edu/teams/rings/status.html*

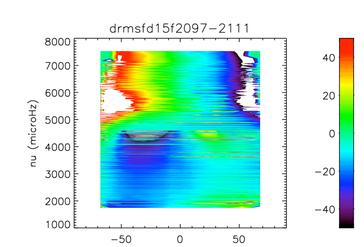

Fig. 4: Variation in mode frequencies for a fixed set of modes, as a function of frequency and Stonyhurst longitude along the equator, averaged over the first 15 rotations of available HMI data. Note how the east-west asymmetry in mode frequencies reverses between low and high frequencies; the reversal occurs somewhat below the acoustic cutoff frequency.